CHANNEL TEMPERATURE DETERMINATION OF HEMT IN QUASI-STATIC OPERATION

M. Florovič*[1], R. Szobolovszký[1], J. Kováč, jr.[1], J. Kováč[1], A. Chvála[1],
J.-C. Jacquet[2], S. L. Delage[2]

[1]Institute of Electronics and Photonics, FEEIT SUT, Ilkovičova 3, Bratislava, Slovakia
[2]III-V Lab, Route de Nozay, 91460 Marcoussis, France
e-mail: martin.florovic@stuba.sk

Abstract *In this work an average channel temperature determination of HEMT is investigated by utilizing measured quasi-static transfer I-V characteristics and differential recurrent calculations. This method takes advantage of source resistance, threshold voltage and saturation velocity temperature dependence determined using low-power output and transfer I-V characteristics. The channel average temperature dependence on dissipated power for investigated HEMT is calculated and compared with simulation results.*

Keywords HEMT, GaN, quasi-static I-V characteristics, channel temperature

1. INTRODUCTION

The high performance of advanced GaN-based devices is deteriorated by self-heating during the power HEMT operation which has negative influence on the device electrical parameters and reliability [1]. The thermal conductance of substrates plays significant role in the heat dissipation [2]. Various experimental methods essential for complex characterization were developed to determine channel temperature, e.g. Raman spectroscopy or interferometric mapping [3-4].

This work deals with differential method based on quasi-static I-V characterization and subsequently applied to determine the InAlGaN/GaN/SiC HEMT channel temperature. This method is possible to be utilized as well on different structures to investigate the thermal and electrical properties.

2. THEORY

The investigated HEMT equivalent circuit comprises the core HEMT under the gate. The rest of the circuit consists of extrinsic ungated gap area of source to gate channel resistance R_S, drain to gate channel resistance R_D and ohmic contact source/drain area resistance R_C. Under the drain-side gate edge the pinch-off area is formed resulting in a voltage drop V_{PO} in saturation regime. For negligible electric capacitance the difference between the investigated HEMT gate voltage V_{GS} and core HEMT gate voltage V_{GO} is determined by resistance $R_{SX} = R_S + R_C$ and therefore:

$$V_{GS} - V_{GO} = R_{SX} I_D \quad (1)$$

At the operating point the I_D difference is caused by V_{GO}, V_{DO} and average temperature T_A variation multiplied by core HEMT transconductance g_{GO}, output conductance g_{DO} and thermal coefficient k_{GO}, respectively:

$$dI_D = g_{GO} dV_{GO} + g_{DO} dV_{DO} + k_{GO} dT_A \quad (2)$$

Carrier saturation velocity v_{SAT} and leakage current I_L are assumed temperature dependent only, furthermore low temperature dependence of 2DEG concentration is utilized as well [5]. Those conditions result in drain current thermal change dI_A and zero g_{DO} in saturation regime. If I_D is a function of V_{GO}–V_{TH} using threshold voltage V_{TH} of core HEMT then (2) and differential form of (1) result in:

$$dI_D - dI_A = g_{GO}(dV_{GS} - dV_{TH} - I_D dR_{SX} - R_{SX} dI_D) = g_{GO}(dV_{GO} - dV_{TH}) \quad (3)$$

The infinite thermal conductance of the channel between source and drain contacts under the quasi-static condition is supposed to define the average temperature T_A. Therefore the power density distribution along the channel plays no role. Temperature dependence of R_S, R_C and V_{TH} with thermal coefficients $k_{RS} = dR_S/dT_A$, $k_{RC} = dR_C/dT_A$ and $k_{VTH} = dV_{TH}/dT_A$ are requisite for HEMT channel temperature determination. Threshold voltage V_{TH} is typically acquired from low power transfer I-V characteristics [6] whereas R_S and R_C are commonly obtained using transmission line method (TLM) measurements. Due to the finite current saturation level a correction factor r at T_A is essential and is defined as ratio between R_S, R_C at operating I_D and R_S, R_C obtained at low I_D. The self-heating error at operating I_D is advised to be eliminated utilizing thermal simulations or pulsed measurements for accurate r determination. Core HEMT (I_{LO}) and extrinsic leakage current (I_{LE}) are approximated utilizing the leakage current spatial distribution. Temperature variation of I_{LO} and v_{SAT} plays role in $dI_A \approx I_D(dv_{SAT}/v_{SAT}) + dI_{LO}$ whereas I_{LE} is combined with dI_D and substituted in (3) by dI_D–dI_{LE}.

Transfer I-V characteristics measured in saturation regime at two proximate V_{DS} values of difference dV_{DS}^* with consequent dI_D^* are utilized to obtain HEMT output conductance $g_D = dI_D^*/dV_{DS}^*$ at defined V_{GS}. In this case electrical parameters change dI_D^*, dI_A^*, dR_{SX}^*, dV_{GS}^*, dV_{GO}^*, dV_{TH}^*, dR_{SX}^* at the operating point which is defined by V_{DS}, V_{GS}, I_D, R_{SX} is described by the following equation analogous to (3):

$$dI_D^* - dI_A^* = g_{GO}(dV_{GS}^* - dV_{TH}^* - I_D dR_{SX}^* - R_{SX} dI_D^*) = g_{GO}(dV_{GO}^* - dV_{TH}^*) \quad (4)$$

If dI_D is set by dV_{GS} at constant V_{DS} as shown in (3) and (4) defines dI_D^* set by dV_{DS}^* at constant V_{GS}, then $dV_{TH} = dV_{TH}^* = k_{VTH} dT_A$, $dR_{SX} = dR_{SX}^* = k_{RSX} dT_A$ are used in (3) and (4) for the same dissipated power change $dP = V_{DS} dI_D \approx V_{DS} dI_D^* + I_D dV_{DS}^* = dP^*$. Dividing the linearly independent (4) by (3) leads to the solution valid in the saturation regime:

$$-(dV_{TH} + I_D dR_{SX}) - dI_A\left[R_{SX} - \frac{dV_{GS}}{dI_D}\left(1 + \frac{g_D V_{DS}}{I_D}\right)\right] = \frac{g_D V_{DS}}{I_D} dV_{GS} \quad (5)$$

Variables dR_{SX}, dV_{TH} and dI_A employed in (5) are linearly dependent on dT_A.

3. EXPERIMENTAL

The investigated $In_{0.18}Al_{0.80}Ga_{0.08}N$/AlN/GaN HEMT structure was grown on SiC substrate prepared by MOVPE. Top ohmic drain, source and gate contacts were created by standard metallization and soldered to CuMo lead frame with AuSn. The horizontal HEMT dimensions are following: gate width ~ 125 µm, gate length ~ 1 µm, source/drain ohmic contact length ~ 5 µm and ungated area length ~ 5 µm. The whole structure was placed on an Al thermal chuck during measurements.

Quasi-static I-V characteristics were measured using semiconductor parameter analyzer Agilent 4155C and controlled thermal chuck. To obtain I_D and g_D dependence V_{DS} was kept at proximate values 30 V and 28 V while V_{GS} was varied from –3 V to +2 V.

The parameters R_S, R_C, r and V_{TH} were acquired from TLM measurements, low-power output and transfer I-V characteristics at temperature range of 25 – 120°C. 3-D thermal FEM simulations of the device were performed by Synopsys TCAD Sentaurus [7]. The device was recovered by white LED illumination for one minute after each measurement.

4. RESULTS AND DISCUSSION

The measured temperature dependences of R_S and V_{TH} are shown in Fig. 1a. In Fig. 1b are depicted the measured I_D and calculated g_D dependence on V_{GS}. The constant $R_C \approx 1.4\ \Omega$ and R_S dependence on T_A and I_D were determined from TLM measurements. Correction coefficient $r \approx 1+5\text{A}^{-1}I_D$ for R_S at operating temperature and current range was obtained using thermal simulations to eliminate self-heating part. Temperature dependence linearization at low I_D allows to calculate $R_S(I_D\rightarrow 0) \approx 17.5\ \Omega$ at 25 °C, $k_{RS}(I_D\rightarrow 0) \approx 90.3$ mΩ/K, $k_{VTH} \approx 0.58$ mV/K. Relative saturation velocity change $dv_{SAT}(T)/v_{SAT} = -dT/[T+1700K]$ [5] was used in $dI_A \approx I_D(dv_{SAT}/v_{SAT})$. Pinch-off area length $d_{PO} \approx 100$ nm at $V_{DS} \approx 30$ V was retrieved from electro-thermal model.

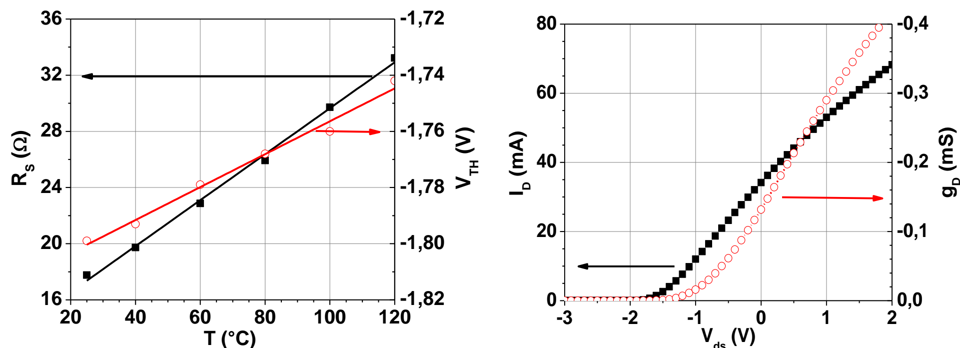

Fig. 1 a) Measured R_S and V_{TH} versus average temperature at low I_D. b) Measured I_D and g_D versus V_{GS} at $V_{DS} \approx 30$ V.

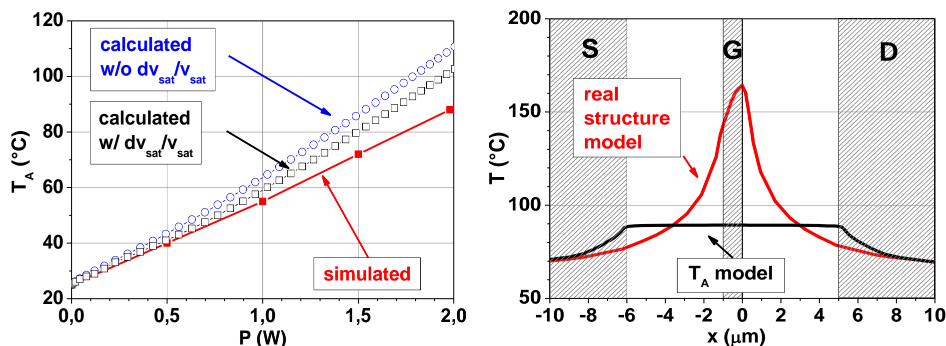

Fig. 2 a) Calculated and simulated average channel temp. T_A versus dissipated power. b) Simulated channel temp. profile for P = 2W (real structure and T_A model).

The calculated T_A shown in Fig. 2a was acquired utilizing (5) in recurrent steps applied to transfer I-V characteristics in the case of included and neglected v_{SAT} change. Consideration of dv_{SAT}/v_{SAT} in calculations results in T_A decrease as shown in Fig. 2a. For I_D < 10 mA constant device thermal resistance was utilized to avoid the uncertainty associated with low g_D and dI_D. Discrepancy in calculated and simulated T_A observed in Fig. 3 for P > 1W is due to major temperature change of R_S. Thus, recurrent calculations (5) describe mostly the average temperature change in the source ungated area. Simulated temperature profile across the channel in the real structure and T_A model including infinite thermal conductance along the channel between drain and source are depicted in Fig. 2b.

5. CONCLUSIONS

Average channel temperature vs. dissipated power of $In_{0.185}Al_{0.815}N/AlN/GaN$ HEMT prepared on SiC substrate was acquired using quasi-static I-V characterization and differential recurrent calculations incrementing V_{GS} at V_{DS} = 30 V. The determination of average channel temperature was affected by mismatch caused by major thermal serial resistance change evident from real structure thermal model. For dissipated power P = 2 W the average channel temperature $T_A \approx 100$ °C was calculated whereas real structure model exhibits maximum temperature $T \approx 168$ °C in the pinch-off area due to high power dissipation. The method demonstrated in this work allows to determine average channel temperature of GaN-based HEMT directly from quasi-static transfer I-V characteristics.

Acknowledgement

The research leading to these results has received from the ECSEL Joint Undertaking (JU) under grant agreement No 783274. The JU receives support from the European Union's Horizon 2020 research and innovation program and France, Germany, Slovakia, Netherlands, Sweden, Italy, Luxembourg, Ireland. The work was also supported by Grant VEGA 1/0739/16 through the Ministry of Education, Science, Research and Sport of Slovakia.

References

[1] O. Ambacher, et. al., *Journal of Appl. Phys.* 85, No. 6, 3222-3233 (1999).

[2] S. Chowdhury, *Phys. Stat. Sol. (A)* 212, Iss. 5, 1066-1074 (2015).

[3] F. Berthet, et. al., *Microel. Rel.* 51, 1796-1800 (2011).

[4] J. Kim, et.al., *Solid-State Electr.* 50, 408-411 (2006).

[5] R. Quay, Dissertation thesis, TU Wien, Ch. 3.2.6 (2001).

[6] M. Florovič, et. al., *Semicond. Sci. Technol.* 32, 025017 (2017).

[7] Sentaurus Device User Guide, v. L-2017.09. Synopsys TCAD Sentaurus, USA, (2017).